Synthesis, Characterization, and Electronic Structure of a New Molybdenum Bronze $SnMo_4O_6$

Dongwoon Jung,*,† Bang-Hee Lee,‡ Sung-Jin Kim,*,‡ and Won Kang§

Department of Chemistry, Wonkwang University, Iksan, Jeonbuk 570-749, Korea, and Departments of Chemistry and Physics, Ewha Womans University, Seoul 120-750, Korea

Received August 11, 2000. Revised Manuscript Received February 6, 2001

$SnMo_4O_6$ was synthesized at low temperature from the mixture of MoO_2 and Mo_2O_3 using Sn flux. The structure of this compound was determined by the single-crystal X-ray diffraction method. It crystallizes in the tetragonal space group $P4/mbm$ with $a = 9.580(4)$ and $c = 2.843(6)$. The structure of $SnMo_4O_6$ is composed of edge-sharing Mo_6O_{12} chains extending down the c axis, and four chains are connected to form channels filled with Sn cations. The resistivity measurement for $SnMo_4O_6$ along the chain direction shows that the compound is metallic down to 50 K, and it exhibits semiconducting behavior as the temperature lowers further. It was found from extended Huckel tight-binding band calculation that the compound is likely to be a quasi-one-dimensional metal. The metal−insulator transition in this compound is due to the Fermi surface nesting phenomenon, which originates in the one-dimensional characteristic.

Introduction

Since the discovery of metal−metal bonded molybdenum bronze $NaMo_4O_6$ by Torardi and McCarley,[1] isostructural ternery molybdenum oxide systems with AMo_4O_6 (A = monovalent cations; K, Rb, In, and Li) and $B_xMo_4O_6$ (B = divalent and trivalent cations; Sn, Pb, Ba, and La; $x < 1$) formulas are successfully synthesized.[2−11] Structurally, all of these compounds are low-dimensional low-valent molybdenum oxides containing Mo_6O_{12}-type octahedral clusters condensed by sharing trans-edges to form infinite chains. Four adjacent chains are perpendicularly bridged by oxygen atoms to form a square channel, which is filled by either mono-, di-, or trivalent cations. The size of channels is slightly oversized; therefore, order−disorder behavior on the cation sites is observed. When divalent or trivalent cations are replaced by monovalent ones, the cationic sites are not completely occupied due to the $B^{2+}-B^{2+}$ or $B^{3+}-B^{3+}$ repulsion as found in $Sn_{0.9}Mo_4O_6$, $Pb_{0.75}Mo_4O_6$, $Ba_{0.62}Mo_4O_6$,[1,2,4,8,12] and $La_{1.16}Mo_8O_{16}$.[13] Consequently, complicated superstructures and distortions on Mo_4O_6 chains that originate from the ordering of the cationic vacancies are observed. For example, $Ba_{0.62}Mo_4O_6$ possesses a superstructure whose true c-axial length is 8 times that of the subcell. The true structure of $La_{1.16}Mo_8O_{16}$ is found to be incommensurate to minimizing the $La^{3+}-La^{3+}$ repulsion. For this reason any stoichiometric compound $B_1Mo_4O_6$ whose cation sites are fully occupied with divalent or trivalent cations has not been reported so far.

There has been a great deal of theoretical investigations in low-dimensional molybdenum oxides to understand their interesting charge-density-wave (CDW) phenomena, anisotropic electrical and magnetic properties. For example, the electronic structures of red bronze $A_{0.33}MoO_3$ (A = Li, K, Rb, Cs, and Tl),[14] magneli phases Mo_4O_{11}[15] and Mo_8O_{23},[16,17] blue bronze $A_{0.3}MoO_3$ (A = K, Rb, and Tl),[18] purple bronze $A_{0.9}Mo_8O_{17}$ (A = Li, Na, K, and Tl),[19,20] and rare-earth bronze $La_2Mo_2O_7$[21] have

* To whom correspondence should be addressed.
† Wonkwang University.
‡ Department of Chemistry, Ewha Womans University.
§ Department of Physics, Ewha Womans University.

(1) Torardi, C. C.; McCarley, R. E. *J. Am. Chem. Soc.* **1979**, *101*, 3963.
(2) Torardi, C. C.; McCarley, R. E. *J. Solid State Chem.* **1981**, *37*, 393.
(3) McCarley, R. E. *Polyhedron* **1986**, *5*, 51.
(4) McCarley, R. E. *Inorganic Chemistry: Toward the 21st Century;* Chisholm, M. H., Ed.; ACS Symposium Series 211; American Chemical Society: Washington, D.C., 1983; pp 274−290.
(5) McCarley, R. E.; Lii, K.-H.; Edwards, P. A.; Brough, L. F. *J. Solid State Chem.* **1985**, *57*, 17.
(6) Torardi, C. C.; McCarley, R. E. *J. Less Common Met.* **1986**, *116*, 169.
(7) Ramanujachary, K. V.; Greenblatt, M.; Jones, E. B.; McCarroll, W. H. *J. Solid State Chem.* **1993**, *102*, 69.
(8) Hoffman, R.; Hoppe, R.; Bauer, K.; Range, K.-J. *J. Less Common Met.* **1990**, *161*, 279.
(9) Chisholm, M. H. *Early Transition Metal Clusters with p-Donor Ligands*; VCH Publishers: New York, 1994; p 1.
(10) Ganne, M.; Baumaza, A.; Dion, M. *Mater. Res. Bull.* **1985**, *20*, 1297.
(11) Travaglini, G.; Wachter, P.; Marcus, J.; Schlenker, C. *J. Solid State Commun.* **1981**, *37*, 599.
(12) Greenblatt, M.; Vincent, H.; Marezio, M. *Low-Dimensional Properties of Molybdenum Bronzes and Oxides*; Schlenker, C., Ed; Kluwer: Amsterdam, 1989.
(13) Leligny, H.; Labbe, Ph.; Ledesert, M.; Raveau, B.; Valdez, C.; McCarroll, W. H. *Acta Crystallogr.* **1992**, *B48*, 134.
(14) (a) Whangbo, M.-H.; Evain, M.; Canadell, E.; Ganne, M. *Inorg. Chem.* **1989**, *28*, 267. (b) Canadell, E.; Whangbo, M.-H. *Inorg. Chem.* **1988**, *27*, 228.
(15) Canadell, E.; Whangbo, M.-H.; Schlenker, C.; Escribe-Filippini, C. *Inorg. Chem.* **1989**, *28*, 1466.
(16) Sato, M.; Nakao, K.; Hoshino, S. *J. Phys. C* **1984**, *17*, L817.
(17) Sato, M.; Fujishita, H.; Sato, S.; Hoshino, S. *J. Phys. C* **1986**, *19*, 3059.
(18) Whangbo, M.-H.; Schneemeyer, L. F. *Inorg. Chem.* **1986**, *25*, 2424.
(19) Whangbo, M.-H.; Canadell, E.; Schlenker, C. *J. Am. Chem. Soc.* **1987**, *109*, 6308.
(20) Whangbo, M.-H.; Canadell, E.; Schlenker, C. *J. Am. Chem. Soc.* **1988**, *110*, 358.
(21) Whangbo, M.-H.; Canadell, E. *Inorg. Chem.* **1987**, *26*, 842.

10.1021/cm000646q CCC: $20.00
Published on Web 04/07/2001

been studied on the basis of their crystal structures. As a result, the origin of the physical properties of these classical molybdenum oxides is well understood.[22] However, very few research activities have been carried out to examine the physical properties of AMo_4O_6 compounds.[23] In discussing the structural and electronic properties of molybdenum oxide metals, it is important to analyze how the Mo atoms possessing d electrons can be identified on the basis of their crystal structures, the d-orbitals of such Mo atoms contributing to the formation of the highest occupied bands, and what kind of dispersion relations and Fermi surfaces are related to their electronic instabilities. In the AMo_4O_6-type family, the variations in their physical properties also mainly originate from the modulation of Mo−Mo interactions. The nature of Mo−Mo bonding in Mo_4O_6 chains are studied on the basis of the bond distance−bond order. For example, when metal cluster electrons (MCEs) are 13 per Mo_4O_6 repeat unit as found in $NaMo_4O_6$, the Mo−Mo bonds in the Mo_4O_6 chain are not distorted. On the other hand, when the MCEs are more than 13 as in KMo_4O_6, the Mo chains undergo distortions with alternating short and long Mo−Mo bonds. Theoretical studies suggest that the observed structural distortions in these molybdenum infinite chains are electronically driven and enhance the Mo−Mo interactions.[24,25]

The modulation of the metal chains seems to affect electronic transport properties. In the present work, we report the synthesis and characterization of a new stoichiometric molybdenum oxide bronze with divalent cation, $SnMo_4O_6$, and examine the electronic structure of this compound on the basis of the crystal structure.

Experimental Section

Synthesis. $SnMo_4O_6$ was synthesized by heating the mixture of MoO_2 (Aldrich 99%) and Mo_2O_3 (Aldrich 99.5%) with an excess amount of element Sn (Aldrich 99.9%) as a flux. The mixed ratio of the starting mixture was MoO_2:Mo_2O_3:Sn = 3:1:10. The reaction mixture was flame sealed in evacuated double quartz tubes 9 and 13 mm in diameter and heated at 850 °C for 2 weeks and then cooled to 300 °C at a cooling rate of 10 °C/h. The silvery needle shape crystals were separated from Sn flux.

Physical Measurements. Electrical resistivity of needle-shaped crystals with ~3-mm length was measured using the standard four-probe method. Four 20-μm wires were connected to the sample by silver paste. A low-frequency lock-in technique was adopted to measure the resistivity. Semiquantitative composition analysis of the compound was performed by an electron-dispersive X-ray (EDX) using a scanning electron microscope (SEM-Philips XL20, EDX-PV9900).

Crystallographic Studies. A silvery needle-shaped crystal was mounted on a glass fiber. Preliminary examination and data collection was performed with Mo Kα_1 radiation (λ = 0.71073) on a four-circle single diffractometer (Enraf-Nonius CAD4) equipped with an incident beam monochromator graphite crystal. The unit cell parameters and the orientation matrix for data collection were obtained from the least-squares refinement, using setting angles of 25 reflections in the range of 17° < 2θ < 28°. No evidence of superstructure reflections was found in larger crystals along every crystal axis. The subsequent refinements confirmed the choice of a third space group. Intensity data were collected with the ω−2θ technique. The intensities of two standard reflections measured every 100 reflections showed no significant deviations during the data collection. The intial positions for all atoms were obtained from the direct methods of the SHELXS-86 program. The structure was refined by the full-matrix least-squares technique with the use of the SHELXS-93 program. Anisotropic thermal motions were included. The final cycle of refinement performed on F_o^2 with 154 unique reflections afforded residuals R1 ($F_o^2 > 0$) = 0.447. Difference Fourier calculations with the phase based on the final parameters showed no peak greater than 10% of the height of an O atom.

Electronic Structure Calculations. We carried out tight-binding band electronic structure calculations based upon the extended Hückel method[26,27] to investigate the properties of $SnMo_4O_6$. The PC version of the CAESAR program was used for the calculations. Atomic parameters used in the calculations are shown in Table 1.

Table 1. Atomic Parameters Used in EHTB Calculations[a]: Valence Orbital Ionization Potential H_{ii}(eV) and Exponent of the Slater-Type Orbital ζ

atom	orbital	H_{ii}	ζ_1 (c_1)	ζ_2 (c_2)
Mo	4d	−10.50	4.54 (0.5899)	1.90 (0.5899)
	5s	−8.34	1.96	
	5p	−5.24	1.90	
O	2s	−32.3	2.275	
	2p	−14.8	2.275	

[a] Parameters are collected from the following data: (a) Clementi, E.; Roetti, C. *Atom. Data Nucl. Data Tables* **1974**, *14*, 177. (b) McLeen, A. D.; McLeen, R. S. *Atom. Data Nucl. Data Tables* **1981**, *26*, 197. (c) Richardson, J. W.; Blackman, M. J.; Ranochak, J. E. *J. Chem. Phys.* **1973**, *58*, 3010.

Table 2. Crystal Data and Structure Refinement for $SnMo_4O_6$

empirical formula	$SnMo_4O_6$
formula weight	422.57
temperature, K	293(2) K
wavelength, Å	0.71073 Å
crystal system	tetragonal
space group	*P*4/*mbm*
unit cell dimensions, Å	a = 9.5804(9) b = 9.5804(9) c = 2.8436(4)
volume, Å^3	261.00(5)
Z	2
density (calculated)	5.398 mg/m^3
absorption coefficient	4.727 mm^{-1}
θ range for data collection	3.01°−24.85°
independent reflections	154 [R(int) = 0.00]
data/restraints/parameters	154/0/22
final R indices [$I > 2\sigma(I)$]	R_1 = 0.163. wR_2 = 0.0447
R indices (all data)	R_1 = 0.163. wR_2 = 0.0447
largest diff. peak and hole	0.806 and −0.763 e/Å^3

Results and Discussion

Crystallographic data for $SnMo_4O_6$ are given in Table 2. The observed Laue symmetry and systematic extinctions led us to choose the space group *P*4/*mbm* (No. 127) for the compound. The tetragonal unit cell parameters and calculated volume were a = 9.5804(9), c = 2.8436(4), and V = 261.00(5). Table 3 lists the positional parameters and equivalent isotropic thermal parameters for $SnMo_4O_6$. The crystal structure of $SnMo_4O_6$ is closely related to those of $NaMo_4O_6$ and KMo_4O_6 in terms of the lattice type and Mo−O bond distances. However, the cation−oxygen distance is shorter in $SnMo_4O_6$ (i.e., Sn−O; 2.294 Å) than in other isostruc-

(22) Whangbo, M.-H.; Canadell, E. *Acc. Chem. Res.* **1989**, *22*, 375.
(23) Kang, D.-B. *Bull. Kor. Chem. Soc.* **1995**, *16*, 929.
(24) Bond, M. R.; Hughbanks, T. *Inorg. Chem.* **1992**, *31*, 5105.
(25) Hughbanks, T.; Hoffman, R. *J. Am. Chem. Soc.* **1983**, *105*, 3528.
(26) Ammeter, J. H.; Bürgi, H.-B.; Thibeault, J.; Hoffmann, R. *J. Am. Chem. Soc.* **1978**, *100*, 3686.
(27) Whangbo, M.-H.; Hoffmann, R. *J. Am. Chem. Soc.* **1978**, *100*, 6093.

Table 3. Atomic Coordinates ($\times 10^{-4}$) and Equivalent Isotropic Displacement Parameters ($Å^2 \times 10^{-3}$) for $SnMo_4O_6$

	x	*y*	*z*	*U*(eq)[a]
Sn(1)	0	0	0	9(1)
Mo(1)	3979(1)	1021(1)	0	4(1)
Mo(2)	6446(1)	1446(1)	−5000	9(1)
O(1)	2927(5)	2073(5)	−5000	7(2)
O(2)	2359(5)	−412(5)	0	10(2)

[a] *U*(eq) is defined as one-third of the trace of the orthogonalized U_{ij} tensor.

Table 4. Bond Lengths [Å] and Angles [deg] for $SnMo_4O_6$[a]

Sn(1)−O(2)	2.294(5)
Sn(1)−Sn(1)	2.8436(4)
Mo(1)−O(1)	2.014(5)
Mo(1)−O(2)	2.072(5)
Mo(1)−Mo(1)	2.765(2)
Mo(1)−Mo(2)	2.7879(8)
Mo(1)−Mo(1)#5	2.8436(4)
Mo(2)−O(1)#9	2.006(7)
Mo(2)−O(2)#7	2.077(4)
Mo(2)−Mo(1)#8	2.7879(8)
Mo(2)−Mo(1)#5	2.7879(8)
Mo(2)−Mo(1)#7	2.7879(8)
Mo(2)−Mo(2)#4	2.8436(4)
Mo(2)−Mo(2)#5	2.8436(4)
O(2)#1−Sn(1)−O(2)#2	90.0
O(2)#2−Sn(1)−O(2)	180.0
O(2)#1−Sn(1)−Sn(1)#4	90.0
Sn(1)#4−Sn(1)−Sn(1)#5	180.0
O(2)−Mo(1)−Mo(1)#4	90.0
Mo(1)#7−Mo(1)−Mo(1)#4	90.0

[a] Symmetry transformations used to generate equivalent atoms: (#1) $y, -x, -z$; (#2) $-x, -y, -z$; (#3) $-y, x, z$; (#4) $x, y, z+1$; (#5) $x, y, z-1$; (#6) $-y+1/2, -x+1/2, z$; (#7) $-x+1, -y, -z$; (#8) $-x+1, -y, -z-1$; (#9) $-y+1, x, z$; (#10) $-y+1/2, -x+1/2, z-1$; (#11) $y, -x+1, -z-1$.

Table 5. Anisotropic Displacement Parameters ($Å^2 \times 10^{-3}$) for $SnMo_4O_6$[a]

	U_{11}	U_{22}	U_{33}	U_{23}	U_{13}	U_{12}
Sn(1)	10(1)	10(1)	7(1)	0	0	0
Mo(1)	4(1)	4(1)	4(1)	0	0	0(1)
Mo(2)	3(1)	3(1)	21(1)	0	0	0(1)
O(1)	8(2)	8(2)	7(3)	0	0	0(3)
O(2)	8(2)	10(3)	10(2)	0	0	−3(2)

[a] The anisotropic displacement factor exponent takes the form $-2p^2[h^2a^{*2}U_{11} + \ldots + 2hka^*b^*U_{12}]$.

tural compounds (i.e., K−O; 2.770 Å in KMo_4O_6 and Na−O; 2.74 Å in $NaMo_4O_6$). The Mo−Mo bond distances are also slightly shorter in $SnMo_4O_6$ (i.e., 2.765, 2.788, and 2.843 Å) than those in KMo_4O_6 (i.e., 2.754, 2.774, 2.794, and 2.879 Å), which results in the displacements of the bridging oxygen atoms closer toward the central cation. The selected bond distances and angles are listed in Table 4. The complete tables of lengths and angles for the compound are available.

The perspective view of the crystal structure of $SnMo_4O_6$ is illustrated in Figure 1 in which the metal−metal bonded infinite chains and square channels are clearly shown. A projection view of the two-dimensional chain structure along the *c* axis is shown with atomic labels in Figure 2. In the projection view, the rectangular units, which are composed of Mo−O and Mo−Mo bonds, are connected through bridging oxygens in the form that one rectangular is perpendicular to the next one. Four rectangular units are bonded through oxygens to construct a channel in which the cations sit. In reality

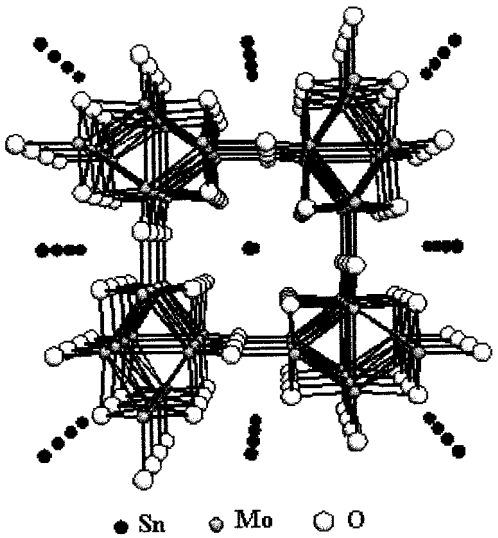

Figure 1. Perspective view of the structure of $SnMo_4O_6$.

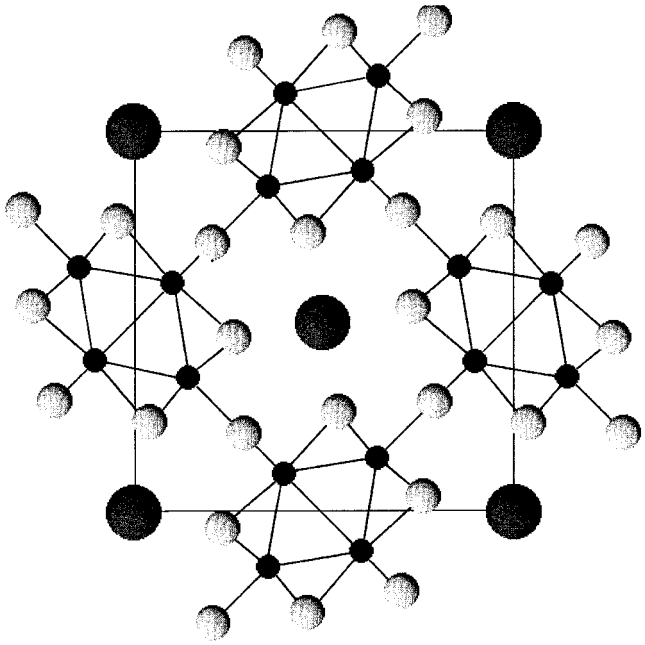

Figure 2. Projection view of the two-dimensional chain structure of $SnMo_4O_6$. Large black circles, small black circles, and gray circles represent Sn, Mo, and O, respectively. The two-dimensional unit cell in the *xy* plane is shown with the solid line.

two Mo atoms forming an acute angle (Mo-1) are positioned behind by 1/2*c* compared with those forming an obtuse angle (Mo-2) in a rectangular unit. Consequently, the Mo−Mo bonds are formed between Mo-2 and Mo-1, and four Mo-2 and two Mo-1 construct a distorted Mo_6 octahedron, which is edge-shared with the next one along the *c* direction.

The electrical resistivity along the crystallographic *c* direction of $SnMo_4O_6$ as a function of temperature is shown in Figure 3. The compound is metallic down to ≈50 K, but it exhibits semiconducting behavior as the temperature goes down further. It is clear from the resistivity data that $SnMo_4O_6$ shows a metal-insulating transition as found in the isostructural KMo_4O_6. The difference in the metal-insulating transition temperature between $SnMo_4O_6$ and KMo_4O_6 may be related to the structural and electronic properties of both com-

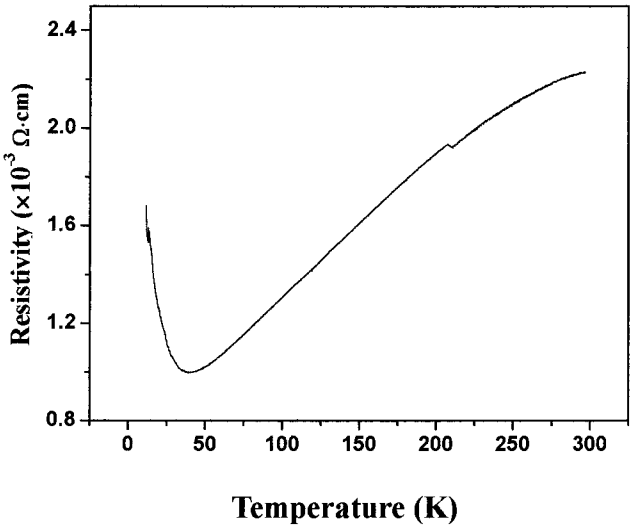

Figure 3. Electrical resistivity data of $SnMo_4O_6$ as a function of temperature.

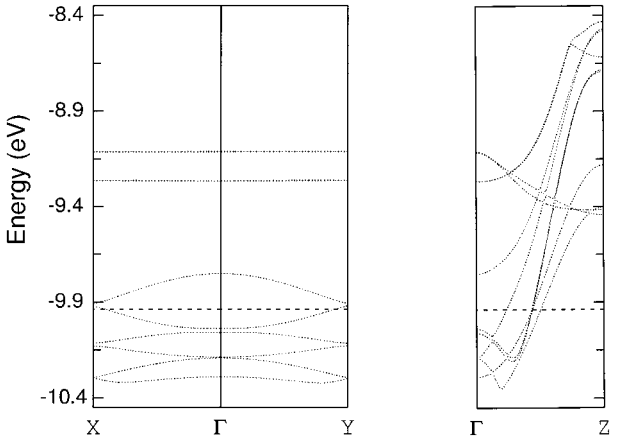

Figure 4. Band dispersions calculated for $SnMo_4O_6$. Dashed line represents the Fermi energy.

pounds. We will continue to study this subject in detail later by performing the crystal structure analyses and electronic structure calculations. The resistivity along the *c* axis for $SnMo_4O_6$ at room temperature is about 2.2×10^{-3} Ω·cm, which is slightly larger than that found for KMo_4O_6. We could not measure the resistivity perpendicular to the *c* axis with the four-probe method because the size of the crystal was too small. Generally, large size crystals are easily obtained in the case of red, blue, and purple bronzes but not in the AMo_4O_6 family.

Band dispersions calculated for $(Mo_8O_{12})^{8-}$ units of $SnMo_4O_6$ are shown in Figure 4 where Γ, *X*, *Y*, and *Z* represent (0,0,0), (π/a,0,0), (0,π/b,0), and (0,0,π/c) in the reciprocal lattice, respectively. The dispersion curves along the *a** and *b** directions are exactly the same because the crystal is tetragonal. The bands are strongly dispersive along the *c** direction while those along the *a** and *b** directions are weakly dispersive. The band dispersion clearly tells us that $SnMo_4O_6$ is said to be a quasi-one-dimensional metal. We rationalize this feature from the crystal structure of $SnMo_4O_6$ that edge-shared perovskite MoO_5 slabs are connected along the *c* direction to make strong Mo−O interactions. More importantly, the Mo−Mo interaction along the *c* direction is supposed to be stronger than those along the other two directions, although the Mo−Mo bond distance along the *c* direction (i.e., 2.843 Å) is larger than the other two Mo−Mo bonds (i.e., 2.765 and 2.843 Å). Electrical conductivity is, therefore, much higher along the *c* axis than the other two directions. Consequently, $SnMo_4O_6$ is a quasi-one-dimensional metal, which is similarly found in the AMo_4O_6 family.

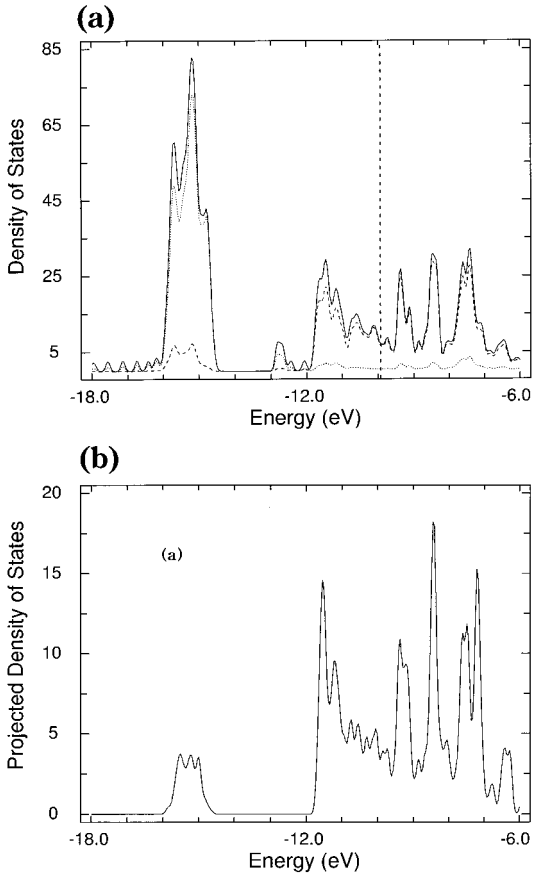

Figure 5. (a) Density-of-states (DOS) curve calculated for $SnMo_4O_6$. Solid line, dashed line, and dotted line represent total DOS, Mo 4d contribution, and O 2p contribution, respectively. (b) Projected density-of-states (PDOS) of the Mo 4d calculated for the 1D chain. * Vertical dashed line represents the Fermi energy.

Figure 5a shows the DOS curve calculated for the three-dimensional $SnMo_4O_6$ structure. In the vicinity of the Fermi energy, which is represented by a vertical dashed line, the orbital contribution from the Mo 4d (see the peaks illustrated by the dashed line in Figure 5a) is very strong while those from the O 2p and Sn 5p are almost zero. This means that electrons in the Mo 4d orbital contribute mainly to the electrical conductivity of $SnMo_4O_6$. Figure 5b is the projected density-of-states (PDOS) of the Mo 4d calculated for the one-dimensional (1D) chain (i.e., calculation along the *c* direction with a rectangular structure including the bridging oxygens as a unit cell). It is clear that the shapes of the Mo 4d PDOS calculated for the 1D chain is almost similar to that shown in Figure 5a (dashed line), which is three-dimensionally calculated. The results illustrate that the intrachain interaction (i.e., interaction along the *c* direction) is much more important than the interchain interaction (i.e., interaction along the *a* and *b* directions). The wide energy region (~5 eV) of the Mo 4d block band shown in Figure 5a,b shows that the Mo−Mo interaction is strong along the *c* direction.

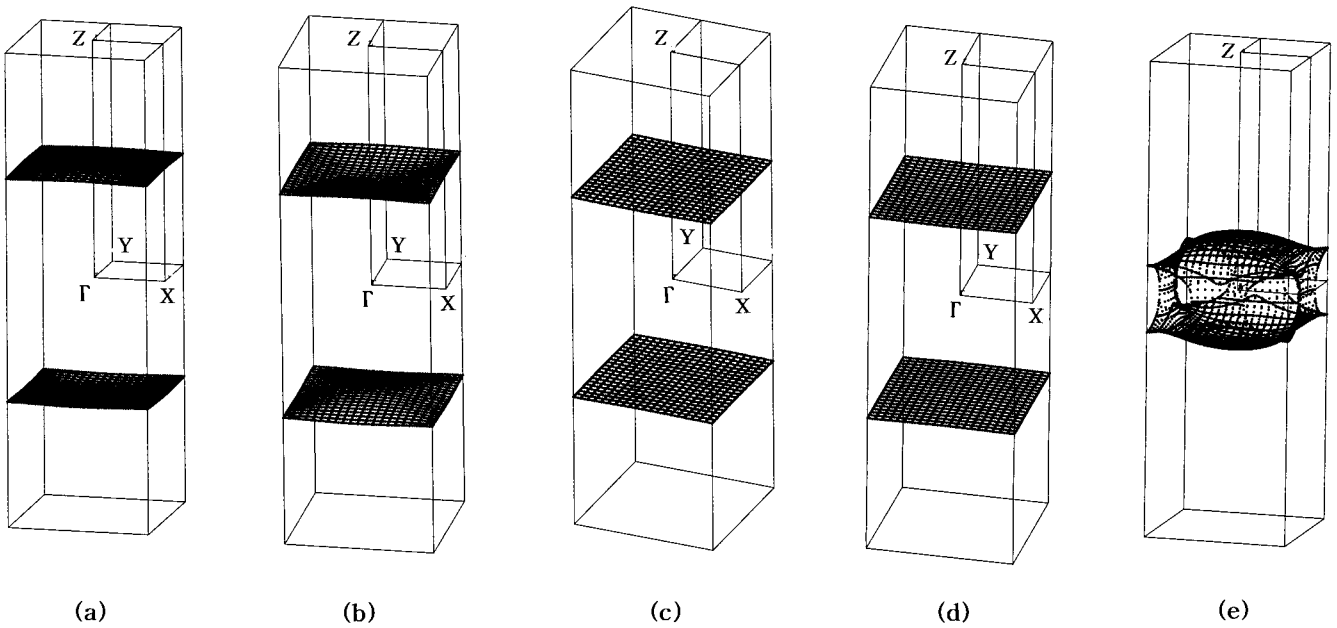

Figure 6. Fermi surfaces associated with the five partially filled bands. (a)−(d) are associated with the lowest four partially filled bands and (e) the highest partially filled band.

A low-dimensional metal is susceptible to becoming an insulator when the temperature is lowered. The electronic instability leading to the metal−insulator transition arises typically when its Fermi surface is nested. A new insulating state comes out as a result of orbital mixing between filled and empty levels in the vicinity of the Fermi energy. Either CDW or spin density wave (SDW) state is obtained depending upon how electrons are filled in new orbitals. Fermi surfaces associated with the partially filled band dispersions of $SnMo_4O_6$ are shown in Figure 6. As already mentioned in the band dispersions, five bands are cut by the Fermi energy. The Fermi surfaces associated with the lowest four bands [see Figure 6a−d] are open along the a^* and b^* directions while they are close along the c^* direction, which means that the electrical conductivity arises only along the c axis. On the other hand, the Fermi surface associated with the highest band [see Figure 6e] shows a three-dimensional nature. Electrons moving along the c^* direction dominate to bring forth the metallic property of the compound. Because the conductivity of a metal is proportional to the number of electrons per unit volume, that along the c^* direction is much higher than those along the other two directions as discussed earlier, and hence $SnMo_4O_6$ possesses 1D character. As found in many compounds exhibiting 1D character, the Fermi surfaces in Figure 6a−d exhibit the partial nesting phenomena with the averaged nesting vector $q \sim 0.5c^*$, which results in the unit cell being enlarged along the c direction over the temperature range below 50 K. Thus, the metal−insulator transition in $SnMo_4O_6$ possibly originates from the Fermi surface nesting in this material. The unnested Fermi surface associated with the highest band may exhibit some metallic character for the compound even after the M−I transition. But when the change in the crystal structure caused by the M−I transition associated with the nested Fermi surfaces is strong enough, the compound after the M−I transition may not have partially filled bands.

Conclusions

$SnMo_4O_6$ was synthesized at low temperature from the mixture of MoO_2 and Mo_2O_3 using Sn flux. The structure of this compound was determined by the single-crystal X-ray diffraction method. It crystallizes in the tetragonal space group $P4/mbm$ with $a = 9.580(4)$ and $c = 2.843(6)$. The structure of $SnMo_4O_6$ composed of edge-sharing Mo_6O_{12} chains extending down the c axis and four chains are connected to form channels filled with Sn cations. The resistivity measurement along the chain direction shows that the compound exhibits metallic property down to 50 K, where a transition to semiconducting behavior occurs. Electronic band structure calculations carried out on the basis of the crystal structure at room temperature show that $SnMo_4O_6$ is a quasi-one-dimensional metal. The strong Mo−Mo interactions along the c axis play an important role for the low-dimensional metallic property of this compound. The metal−insulator transition that occurred at ≈50 K is possibly due to the Fermi surface nesting phenomena that originated from the 1D nature in $SnMo_4O_6$.

Acknowledgment. This work is supported by Korea Research Foundation Grant (KRF-2000-015-DP0224), and partly by Wonkwang University in the program year of 2000. D. Jung wishes to thank professor Whangbo for the invaluable comments.

CM000646Q